minerals

MDPI

Article

The Role of Hydrocarbons in the Formation of Uranium Mineralization, Louzhuangzi District, Southern Junggar Basin (China)

Zhong-Bo He [1,2], Bao-Qun Hu [1,*], Lin-Fei Qiu [2], Yun Wang [1], Hong Chen [3], Wei-Wei Jia [3], Yi-Fei Li [1], Hua-Li Ji [2] and Man-Huai Zhu [1]

[1] State Key Laboratory of Nuclear Resource and Environment, East China University of Technology, Nanchang 330013, China; hzb100029@163.com (Z.-B.H.); wy@ecut.edu.cn (Y.W.); 2023210034@ecut.edu.cn (Y.-F.L.); zmh2022110063@163.com (M.-H.Z.)
[2] CNNC Key Laboratory of Uranium Resource Exploration and Evaluation Technology, Beijing Research Institute of Uranium Geology, Beijing 100029, China; qiulinfei@briug.cn (L.-F.Q.); jhl100029@163.com (H.-L.J.)
[3] No. 216 Nulear Geological Brigade, China National Nuclear Corporation, Urumqi 830011, China; chenhong305@163.com (H.C.); lzz2019216@163.com (W.-W.J.)
* Correspondence: bqhu@ecut.edu.cn

Abstract: In recent years, there have been important breakthroughs in the exploration for sandstone-hosted uranium (U) deposits in the Louzhuangzi district of the southern Junggar Basin. Between 2020 and 2023, a medium-sized sandstone-hosted uranium deposit production area was identified in the region. Only a few investigations have been conducted at the Louzhuangzi U deposit, including those analyzing its geological–tectonic evolution, basic geological features, hydrogeology, and ore-controlling factors. It is generally believed that uranium mineralization at the Louzhuangzi U deposit is controlled by a redox zone. Organic matter (referred to as OM hereafter) consisting of bitumen and carbonaceous debris is very common in the uranium ores (especially in high-grade ores) at the Louzhuangzi U deposit. However, the characteristics of the OM and its contribution to uranium's mineralization have not been studied in detail. In this study, OM-rich U-ores, altered sandstone, and barren sandstone samples were collected for petrography, mineralogical, micro-spectroscopy, carbon, and sulfur isotope studies. The results of this study show that the distribution of U minerals and metal sulfides (pyrite, sphalerite, etc.) was strictly controlled by bitumen at the Louzhuangzi U deposit. The bitumen may have been formed by hydrocarbon-rich and U-rich ore-forming fluids, which were formed after hydrocarbon generation and expulsion in the underlying Jurassic coal-bearing source rocks. The fluids contained U, Zn, Fe, and other metal elements, which migrated together and then precipitated into the oxidized Toutunhe Formation sandstone through cracking and differentiation processes. Therefore, the results indicate that migrated hydrocarbons were involved in U mineralization, in addition to oxidation–reduction processes, in the Louzhuangzi district, south of the Junggar Basin (China).

Keywords: organic matter; hydrocarbon fluids; cracking and differentiation processes; sandstone-hosted uranium deposit; Junggar Basin

check for updates

Citation: He, Z.-B.; Hu, B.-Q.; Qiu, L.-F.; Wang, Y.; Chen, H.; Jia, W.-W.; Li, Y.-F.; Ji, H.-L.; Zhu, M.-H. The Role of Hydrocarbons in the Formation of Uranium Mineralization, Louzhuangzi District, Southern Junggar Basin (China). *Minerals* **2024**, *14*, 709. https://doi.org/10.3390/min14070709

Academic Editors: Raymond H. Johnson and Johanna Blake

Received: 15 May 2024
Revised: 4 July 2024
Accepted: 11 July 2024
Published: 12 July 2024

Copyright: © 2024 by the authors. Licensee MDPI, Basel, Switzerland. This article is an open access article distributed under the terms and conditions of the Creative Commons Attribution (CC BY) license (https://creativecommons.org/licenses/by/4.0/).

1. Introduction

Sandstone-hosted uranium (U) deposits are increasingly recognized as the most promising uranium resources globally, owing to their advantages of large-scale tonnage, low in situ leaching costs, and environmental friendliness [1]. As of 2019, sandstone-hosted U deposits constitute 39.6% of all discovered uranium deposits worldwide, ranking first [2]. Since the 1990s, numerous large and super-large sandstone-hosted U deposits have been uncovered within the Mesozoic–Cenozoic sedimentary basins in Northern China—notably the Yili, Junggar, Ordos, Erlian, and Songliao Basins [3–6]—accounting for

approximately 53% of the uranium resources in China [1]. The Mesozoic Jurassic strata of Xinjiang Province stand out as significant producers of in situ leachable sandstone-hosted U deposits, exemplified by the Mengqiguer, Honghaigou, and Kamusite deposits.

The Junggar Basin, situated in Northwest China, represents a crucial energy-producing region, boasting vast reserves of oil, natural gas, coal, and U. Over the past few decades, extensive drilling programs involving hundreds of drill holes of more than 260,000 m have led to the discovery of numerous U deposits or occurrences within the Junggar Basin, including the Kamusite, Liuhuanggou, Karamay, Beisantai, and Dingshan deposits [7–12]. Extensive scientific investigations have been conducted on various aspects of the geotectonic evolution [13], sedimentological–petrological characteristics [14], geochemical attributes [15], sources of ore-forming materials [16], and metallogenic mechanisms of the sandstone-hosted U deposits in the Junggar Basin [14,17,18].

Among the newly discovered deposits within the southern Junggar Basin, the Louzhuangzi U deposit has the potential to become large-scale. Recent research endeavors have focused on the sedimentary characteristics of the ore-bearing strata, the forms of uranium minerals, the controlling factors of U mineralization, and the metallogenic mechanism [19–21]. Lu et al. proposed that the deposit is influenced by an interlayer oxidation zone [21], globally modeled as U transport, facilitated by oxidizing groundwater within the permeable layers towards the redox boundaries [22]. Notably, the presence of U-rich and U-bearing bitumen in the Louzhuangzi district, coupled with the discovery of an oil production test hole approximately 3 km southwest of the deposit, raises questions regarding the potential contribution of deep hydrocarbon-rich fluids to the uranium mineralization in this district.

The role of organic matter in uranium mineralization has been addressed by many scholars worldwide [23–25], and the reduction and adsorption of organic matter are emphasized in the process of sandstone-hosted U mineralization.

Moreover, many scholars highlight the significant roles of hydrocarbon fluids in sandstone-hosted U mineralization [4,26,27]. Although scholars have identified the widespread existence of bitumen and carbonaceous organic matter at the Louzhuangzi U deposit [21,22], to date, no scientific investigations have explored the relationship between U mineralization and hydrocarbon fluids.

Following a field geological survey, representative samples composed of U-ores, altered rocks, and source rocks were collected from drill holes at the Louzhuangzi U deposit. Subsequent analyses involved petrographic examinations, mineralogical assessments, fluid inclusion studies, and the analysis of trace Earth elements (including rare earth elements) and carbon isotopes using techniques such as optical microscopy, fluorescence microscopy, scanning electron microscopy with energy-dispersive X-ray spectroscopy (SEM-EDX), and micro-laser infrared spectroscopy. This study endeavored to elucidate the characteristics of organic matter and explore the genetic relationship between organic matter composed of carbonaceous debris or hydrocarbon fluids and U mineralization at the Louzhuangzi U deposit in the southern Junggar Basin.

2. Geological Setting

2.1. Tectonic Background

The southern area of the Junggar Basin spans the North Tianshan tectonic zone and the southern fold-fracture zone (Figure 1a) [28,29]. The southern fold-fracture zone unit comprises four secondary tectonic subdivisions: the western fault-fold belt; the Chaiwopu–Dabancheng depression structural belt; the Bogda basement thrust zone; and the Bogda piedmont thrust nappe belt (Figure 1b) [30]. Since the Cenozoic era, the collision and sustained compression between the Eurasian and Indian plates have precipitated robust thrusting and nappe formations within the meso-Cenozoic strata along the southern margin of the Junggar Basin. Consequently, three distinct rows of thrust and fold belts have emerged, extending predominantly in an east–west direction within the western fault-fold belt [31–34]. The Luozhuangzi U deposit is situated in the eastern segment of the western

fault-fold belt, primarily influenced by the Kalaza syncline and Liuhuanggou anticline (Figure 1b,c).

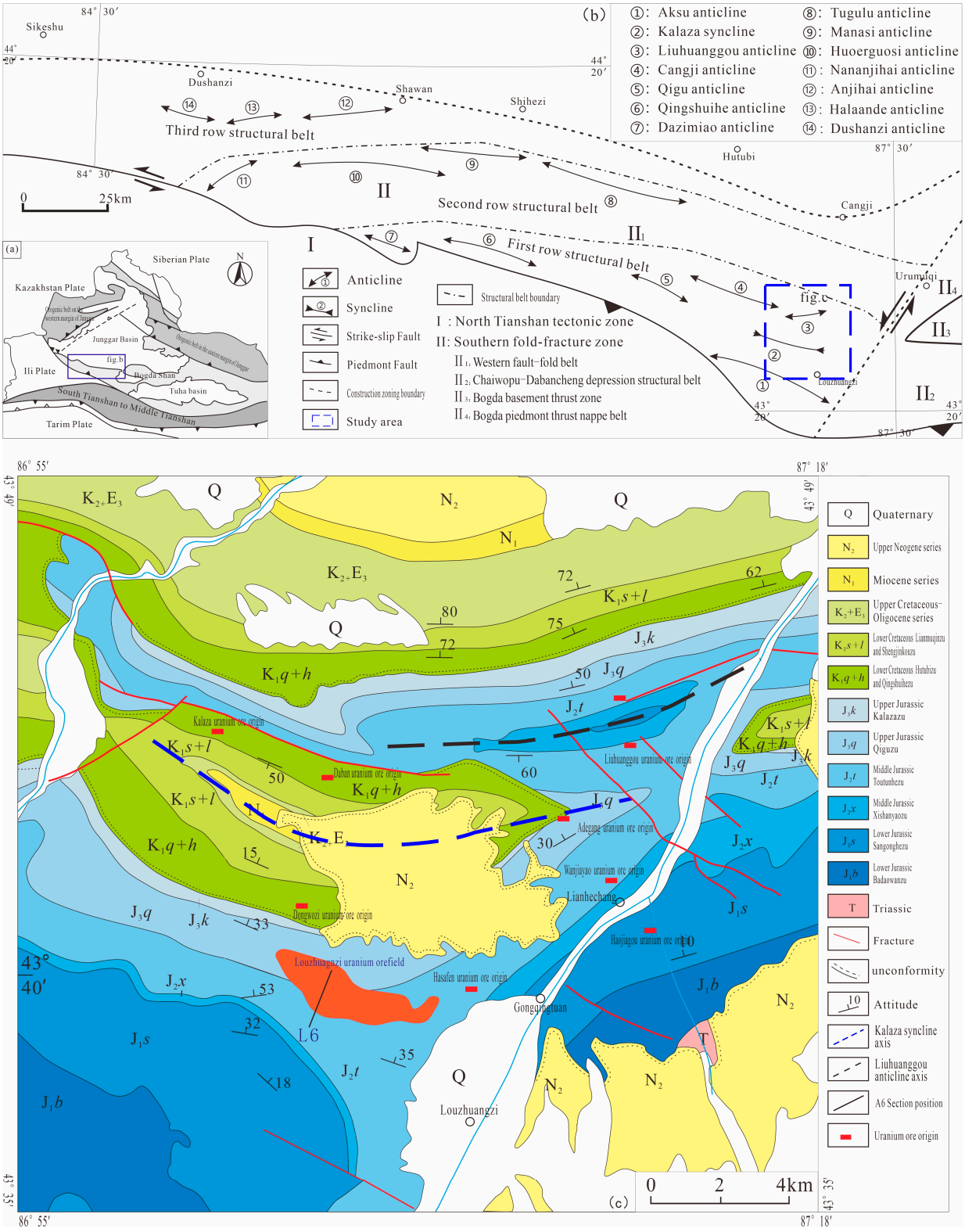


Figure 1. (**a**) Location of the study area; (**b**) map showing tectonic units of the study area, modified from [19,22]; (**c**) geological map of the Louzhuangzi U deposit, modified from [19].

The southern margin of the Junggar Basin has undergone three principal tectogenetic stages from the Mesozoic to the Cenozoic period [29,30]. Initially, during the Indo–China movement, torsional compression occurred, fostering the development of a foreland basin belt along the basin's southern periphery. Subsequently, the Yanshan movement altered the basin's structural configuration, prominently uplifting the surrounding mountainous terrain and shifting the subsidence center's position. Finally, the Himalayan tectonic activity contributed to the establishment of the present configuration, characterized by three east–west-oriented rows of thrust-fault fold belts within the basin (Figure 1b) [29,30].

2.2. Regional Stratigraphy

The study area exhibits diverse stratigraphic sequences spanning from the Mesozoic to the Quaternary periods, encompassing Jurassic, Cretaceous, Paleogene, Neogene, and Quaternary formations (Fm) (Figure 1c). The middle and lower Jurassic Fm are characterized by lake-fluvial facies sedimentation with abundant paleontological fossils, including the Badaowan Fm (J_1b) (coal-bearing), Sangonghe Fm (J_1s), Xishanyao Fm (J_2x) (coal-bearing), and Toutunhe Fm (J_2t). The Upper Jurassic Fm, including the Qigu–Kalaza Formation (J_3q-J_3k), primarily exhibits red variegated sedimentation, indicating an arid–hot paleoclimatic environment (Figure 2).

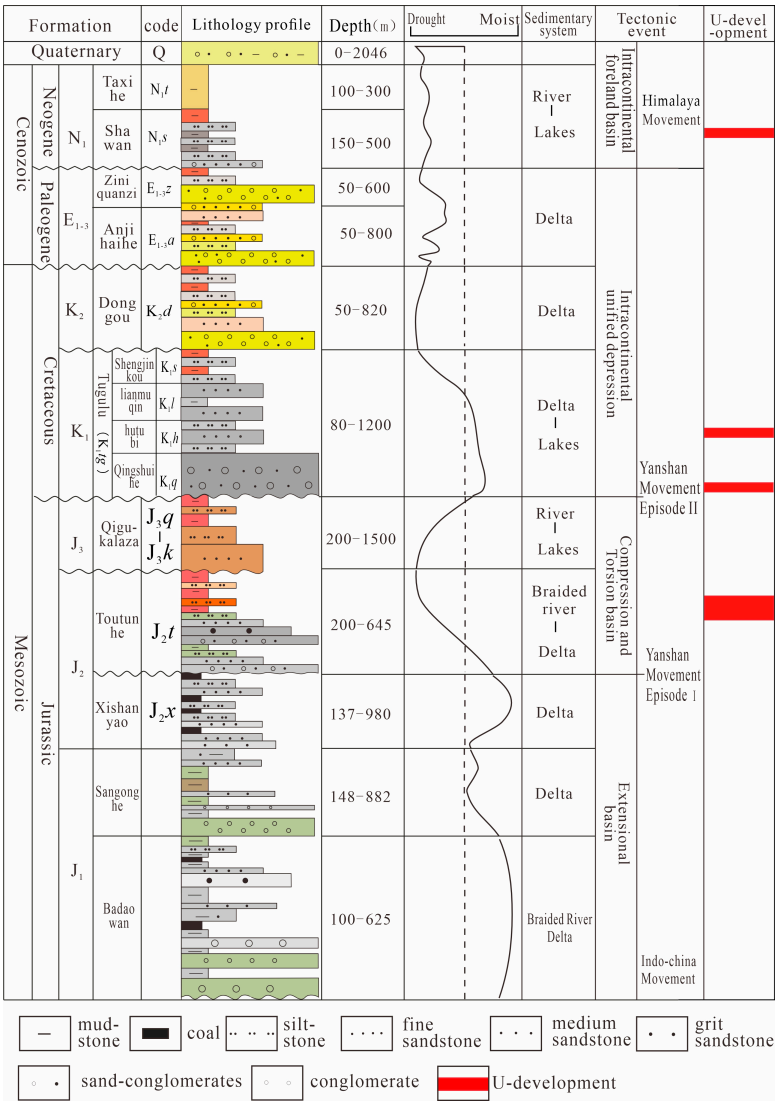


Figure 2. Map showing the comprehensive stratigraphic column of the study area.

The Tugulu Group of the Lower Cretaceous comprises the Qingshuihe Fm, Hutubihe Fm, Shengjinkou Fm, and Lianmuqin Fm. These formations are characterized by deltaic, lacustrine, and fluvial facies sedimentation, consisting predominantly of brownish red, yellow-brown, and gray-green mudstone; sandy mudstone; siltstone; sandstone; and conglomerates with abundant paleontological fossils.

The Donggou Fm (K_2d) of the Upper Cretaceous is typified by gray-white, brown-yellow coarse-grained quartz sandstone, sandstone, and conglomerates interspersed with brown-reddish sandy mudstone. The Paleogene strata include the Anjihaihe Fm ($E_{1\text{-}3}a$) and Ziniquanzi Fm ($E_{1\text{-}3}z$), composed of grayish white, grayish green, and yellowish brown sandstone. The Neogene formations comprise fluvio-lacustrine facies sedimentation within the Shawan Fm and Taxihe Fm.

The Toutunhe Fm of the Middle Jurassic and Cretaceous Qingshuihe and Hutubi Fm represent the primary strata associated with U mineralization in the southern Junggar Basin. Additionally, sandstone-hosted U mineralization is observed to a certain extent within the Neogene Shawan Fm.

2.3. Geological Characteristics of Louzhuangzi U Deposit

The Louzhuangzi U deposit is situated in the eastern segment of the western fault-fold tectonic zone (Figure 1b,c), which is the secondary structural unit in the southern margin of the Junggar Basin. The Toutunhe Fm serves as the primary host stratum for the U-ore bodies in the study area. This formation exhibits a typical rhythmic pattern characterized by gradation in the grain sizes, from coarse at the bottom to finer towards the top, with six rhythmic layers identified in the study area. The lower coarse-grained clastic sedimentary layer appears predominantly gray in color and comprises multiple normal rhythmic layers. Each rhythmic layer lithologically comprises conglomerates, pebbly medium- and fine-grained sandstone, medium- and coarse-grained sandstone, and coarse-grained sandstone, gradually transitioning upwards into gray to gray-green mudstone and siltstone (Figure 2).

The uppermost rhythmic layer of the Toutunhe Fm is characterized by brown and reddish brown interbedded mudstone with the occasional occurrence of gray and gray-green interbedded mudstone. Thin layers of gray and gray-green fine-grained sandstone and medium-grained sandstone are intermittently interspersed within this layer. The distribution of the Toutunhe Fm is governed by the Kalaza syncline and the Liuhuangou anticline. The Louzhuangzi U deposit is situated within the southern wing of the Kalaza syncline, with the strata exhibiting a monoclinal structure inclined towards the northeast. Furthermore, the strata extending towards the eastern turning point gradually incline northwestward, with dip angles ranging between 10° and 25° (Figure 1c) [20].

The controlled U-ore bodies at the Louzhuangzi U deposit extend approximately 4400 m in length along the strike and 200 m to 1000 m in width along the dip. Preliminary investigations indicate that these ore bodies consist of one to three layers, manifesting in tabular and banded formations. All ore bodies are situated within the thick sand body of the third rhythmic layer of the Toutunhe Formation. The thickness of the ore-bearing sand body ranges from 130 m to 190 m, with the ore bodies buried at depths ranging from 33 m to 857 m. The ore body's thickness varies from 1.08 m to 5.6 m, with U-ore grades ranging from 0.011% to 0.094% (Figure 3) [19].

The mineralized sandstones are predominantly gray and gray-white, coarse-grained gravel sandstone, coarse-grained sandstone, and gravel conglomerates. These sandstones exhibit loose or relatively loose cementation and display pronounced kaolinization. Pyrite is commonly observed alongside banded, laminated, and clumped carbonaceous debris. The primary control of the U-ore body lies within the gray and white alteration zone, which extends nearly east–west across the plane. Compared to the barren sandstone, the kaolinization alteration is a prominent feature in the white alteration zone.

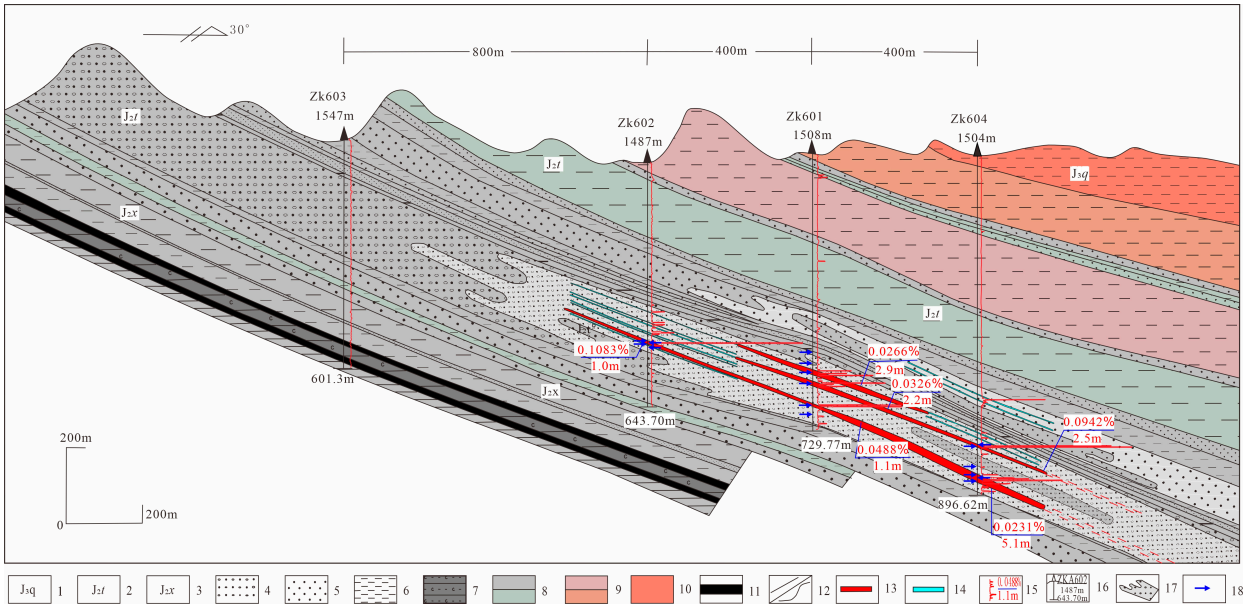


Figure 3. A schematic cross-section (L6) showing the spatial positions of the U-ore bodies considered in this study, modified from [20]. 1—Qigu Fm; 2—Toutunhe Fm; 3—Xishanyao Fm; 4—sand–conglomerate; 5—sandstone; 6—mudstone; 7—gray-blackish carbonaceous mudstone; 8—gray, gray-green color; 9—variegated color; 10—brown color; 11—coal; 12—lithological boundary and formation contact boundary; 13—U-ore body (U% > 0.01%); 14—U-mineralized sandstone; 15—gamma log curve and grade (%) of ore body (m); 16—drill holes with elevation and depth annotations; 17—grayish white alteration zone; 18—sampling location.

3. Sampling, Analytical Procedures, and Methods

3.1. Samples

A total of 27 samples (Table 1) were utilized for this study. All ore samples were collected from drill holes along the L6 cross-section, which was an exploration section in the study area. Additionally, some altered sandstone samples were collected from drill holes ZK1203 and ZK1302, which were located near L6. The direction of the section line was 30 degrees, and the position of the section is shown in Figure 1c. The specific shape of the section is shown in Figure 3. Prior to the laboratory analysis, the samples underwent meticulous observation and photographic documentation. The analytical procedures encompassed mineralogical examinations, quantitative elemental analysis, sulfur isotope analysis of pyrite, carbon isotope analysis, and geochronological investigations.

Table 1. Sample information.

NO.	Sample No.	Lithology	Drill No.	Depth (m)
1	L601-1	Dark gray coarse-grained sandstone	ZK601	528.2
2	L601-2	Dark gray coarse-grained sandstone		556.8
3	L601-3	Gray coarse-grained sandstone (U-ore)		579.3
4	L601-4	Gray coarse-grained sandstone (U-ore)		610.3
5	L601-5	Gray coarse-grained sandstone (U-ore)		667.6
6	L601-6	Gray coarse-grained sandstone		691.6
7	L602-1	Dark gray coarse-grained sandstone (U-ore)	ZK602	472.9
8	L602-2	Gray coarse-grained sandstone (U-ore)		477.5
9	L602-3	Gray coarse-grained sandstone (U-ore)		482.7
10	L602-4	Gray coarse-grained sandstone		490.7

Table 1. *Cont.*

NO.	Sample No.	Lithology	Drill No.	Depth (m)
11	L604-1	Dark gray coarse-grained sandstone (U-ore)	ZK604	766.6
12	L604-2	Dark gray coarse-grained sandstone (U-ore)		772.8
13	L604-3	Gray coarse-grained sandstone		823.7
14	L604-4	Gray coarse-grained sandstone (U-ore)		847.1
15	L604-5	Gray coarse-grained sandstone (U-ore)		854.2
16	L604-6	Dark gray coarse-grained sandstone		863.3
17	L1203-21	Gray coarse-grained sandstone with carbonaceous debris	ZK1203	922.5
18	L1203-24	Coal		978.1
19	L1203-25	Gray coarse-grained sandstone with carbonaceous debris		1010.5
20	L1302-10	Coal	ZK1302	424.6
21	L1302-40	Gray coarse-grained carbonaceous sandstone		676.8
22	L1302-50	Gray coarse-grained carbonaceous sandstone		755.7
23	L1302-54	Gray coarse-grained coal-bearing sandstone		775.8
24	L1302-56	Gray medium-grained sandstone		797.5
25	L1302-57	Gray coarse-grained coal-bearing sandstone		799.2
26	L1302-59	Gray coarse-grained sandstone with carbonaceous debris		809.8
27	L1302-60	Gray coarse-grained carbonaceous sandstone		811.8

3.2. Mineralogical Study

Mineralogical investigations were conducted on 12 ore samples and 5 altered sandstone samples. A microprobe analysis and fluid inclusion studies were performed to elucidate the mineralogical composition and characteristics. These studies were conducted at the laboratory facilities of the Geology and Mineral Resources Division of the Beijing Research Institute of Uranium Geology.

3.2.1. SEM and EPMA

Backscattered electron (BSE) images were acquired using a VEGA3 scanning electron microscope (TESCAN, Brno, Czech Republic). The analytical conditions included 20 kV voltage acceleration. The X-ray energy spectrum analysis was conducted using an EDAX TEAM energy-dispersive spectrometer (EDS, AMETEK, Berwyn, PA, USA), and the parameters included a single-point acquisition time of 200 μs, input CPS of more than 10,000, and dead time of less than 30%. The EPMA was performed on microprobe sections using a JXA-8100 electron microprobe (JEOL, Tokyo, Japan). The analytical conditions included a 15.0 kV accelerating voltage, a 2 μm beam diameter, a counting time of 15 s, and a current of 2.00×10^{-8} A. Calibration was conducted against natural and synthetic oxides or alloys, with detection limits ranging between 0.01% and 0.05%.

3.2.2. Raman Microprobe Spectroscopy

Thin sections were positioned on the stage of a BX-41 microscope (Olympus, Tokyo, Japan) equipped with 10× to 100× objectives, integrated with an evolution-type laser Raman microscope system (HORIBA, Tokyo, Japan). This system included an electronically cooled CCD detector, an illuminant system, and a filter system. Raman spectra were

excited by a 532 nm YAG laser at a resolution of 1 cm^{-1}, and the parameters included a 100× objective, a scanning range between 100 and 4000 cm^{-1}, a grating of 1800 g/mm, a single-point gaining speed of 8 s, and 4 accumulations. The spectra were calibrated using 520.7 cm^{-1} sections of a silicon wafer. Data processing and spectral manipulation, including smoothing, peak analysis, and baseline correction, were executed using Labspec 6 in the Horiba software (Horiba lab spec 6).

3.2.3. Infrared Spectrum Analysis

Infrared spectrum analysis was conducted using the BRUKER LUMOS Micro-FTIR (Billerica, MA, USA) within an ATR model. The analyses consisted of 64 scans with a scanning range between 4000 and 640 cm^{-1} and a resolution of 4 cm^{-1}. Data processing and spectral manipulation were performed using the OPTU 7.5 software as an accessory instrument.

3.3. Quantitative Analysis of Trace Elements

The quantitative analysis of trace elements was conducted on 5 samples of U-ores and 5 unaltered sandstone samples from the primary zone. Twenty-six trace elements (Li, Be, Sc, V, Cr, Co, Ni, Cu, Zn, Ga, Rb, Sr, Y, Mo, Cd, In, Sb, Cs, Ba, W, Tl, Pb, Bi, Th, U) were determined. The samples were processed by crushing them to 200 mesh using ceramic grinding. The concentration of trace elements was measured using the whole-rock dissolution method. Moreover, using the Element XR Inductively Coupled Plasma Mass Spectrometer (ICP-MS) (Thermo Fisher, Waltham, MA, USA), the limit of single-element detection was achieved at 10^{-9}.

3.4. Trace Elements and S Isotope of Pyrite

The trace elements and S isotopes of pyrite in the U-ores were analyzed using the in situ method of femtosecond laser ablation–inductively coupled plasma mass spectrometry (LA-ICPMS, Thermo Fisher, Waltham, MA, USA). During the measurement of the trace elements in pyrite, 31 trace elements (Li, Be, S, Sc, V, Cr, Co, Ni, Cu, Zn, Ga, Ge, As, Rb, Sr, Y, Zr, Nb, Mo, Ag, Cd, In, Sb, Te, Ba, W, Tl, Pb, Bi, Th, U) were determined. Helium was utilized as the carrier gas at a low frequency (6 Hz) to ensure stable signal acquisition. The single-element detection limit was found at 10^{-9} (ppb). The sulfur isotope mass fractionation was corrected via the Standard-Sample Bracketing (SSB) method. The experiment was conducted at Kehui Test (Tianjin) Technology Co., Ltd. (Tianjin, China).

3.5. Carbon Isotope of OM

The carbon isotope analysis of the organic matter in the U-ores was carried out using a system composed of a Flash 2000 element analyzer (Thermo Fisher, Waltham, MA, USA) and a Delta V Plus gas isotope mass spectrometer (Thermo Fisher, Waltham, MA, USA). The OM samples were prepared for extraction by drying the U-ores in an oven for 24 h at 70 °C, followed by wrapping them in a tin cup.

The CO_2 generated in the Flash 2000 Element analyzer was subsequently inserted into the gas isotope mass spectrometer via the application of helium through an online pipeline. The data analysis utilized an SS fused silica capillary column (3 m × 6 mm × 5 mm i.d.) with an oxygen-passing reaction duration of 3 s at a reaction furnace temperature of 960 °C. Helium served as the carrier gas, and CO_2 was the reference gas (GBW04407, GBW04408, and IAEA-600). The standard deviation of the EA-GIMS for each measurement was less than 0.2%.

All experiments were conducted at the Beijing Research Institute of Uranium Geology unless specifically stated otherwise.

4. Results

4.1. Petrography

4.1.1. Organic Matter

In the drill core, the typical U-ores exhibited grayish black, dark gray, and grayish white hues, primarily comprising feldspar sandstone, lithic feldspar sandstone, and a

minor amount of feldspar lithic sandstone (Figure 4). Clastic components mainly consisted of quartz, feldspar, and rock detritus, with a low content of mica and heavy minerals (Figure 4f). Sandstone pores were predominantly filled with calcite and dolomite cementation, while the clastic particles' shapes ranged from secondary corner angles to secondary circles, with medium sorting observed (Figure 4g). Two types of organic matter were found in the U-ores. The first type of OM was widely distributed in the form of fine veins and disseminated within the fracture zones or pore spaces of the sandstone (Figure 4) at a vertical or high angle to the strata (Figure 4a–d). These fine veins could be observed more distinctly under microscopy, presenting a flowing structure indicative of mobility (Figure 4f). The second type of OM was composed of short columnar or fine grains that were dispersed, with typical carbonaceous clastic characteristics (Figure 4e). In the unaltered sandstone of the primary zone, OM was relatively scarce, with scattered fine carbonaceous debris visible in some samples (Figure 4g).

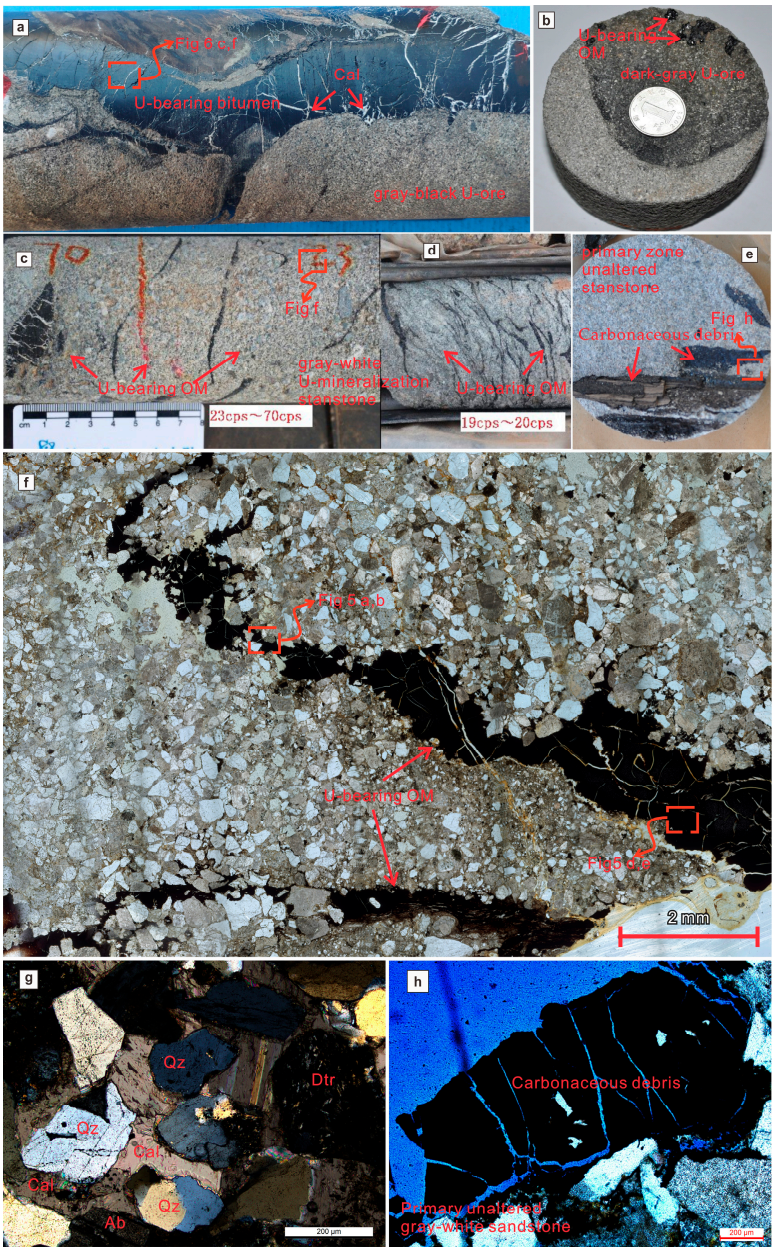


Figure 4. Images showing the macroscopic features of the OM in the U-ores and the primary zone of unaltered sandstone in the Louzhuangzi U deposit. (**a**–**d**) The different color specimens of OM-bearing

U-ores; (**e**) carbonaceous debris in grayish white unaltered (barren) sandstone; (**f**) a mosaic of images showing the microscopic features of fine-veined disseminated OM in a U-ore; (**g**) an image showing the clastic mineral structure of the ore-bearing sandstone and the cementation in its pores; (**h**) an image showing the carbonaceous debris in the unaltered sandstones of the primary zone. OM in U-ore. OM = organic matter; Qz = quartz; Cal = calcite; Dtr = rock detritus; Ab = albite.

4.1.2. Uranium Minerals

Two primary types of U minerals, pitchblende and coffinite, were identified through SEM-EDS and EPMA, both symbiotic with OM (bitumen), pyrite, and sphalerite, among others (Figure 5). U minerals occurred in two forms: dispersed within bitumen as very fine mineral aggregates resembling cloudiness (Figure 5), with particle sizes of mainly less than 1 μm (Figure 5a–e,h); and as irregular clumps situated in the interstitial positions of various mineral particles, with the particle sizes of the blocky pitchblende mainly ranging from 3 to 5 μm, occasionally reaching 10 μm, and predominantly filling the intergranular pores of the sandstone (Figure 5f,i). These observations indicate the close symbiosis of the pitchblende or coffinite with pyrite, OM (bitumen), and sphalerite, primarily controlled by bitumen (Figure 5e,g,h,j). At least two stages of pyrite were present in the U-ores (Py1—the core position; Py2—the growth zone around the core position), with U closely associated with Py2 (Figure 5f).

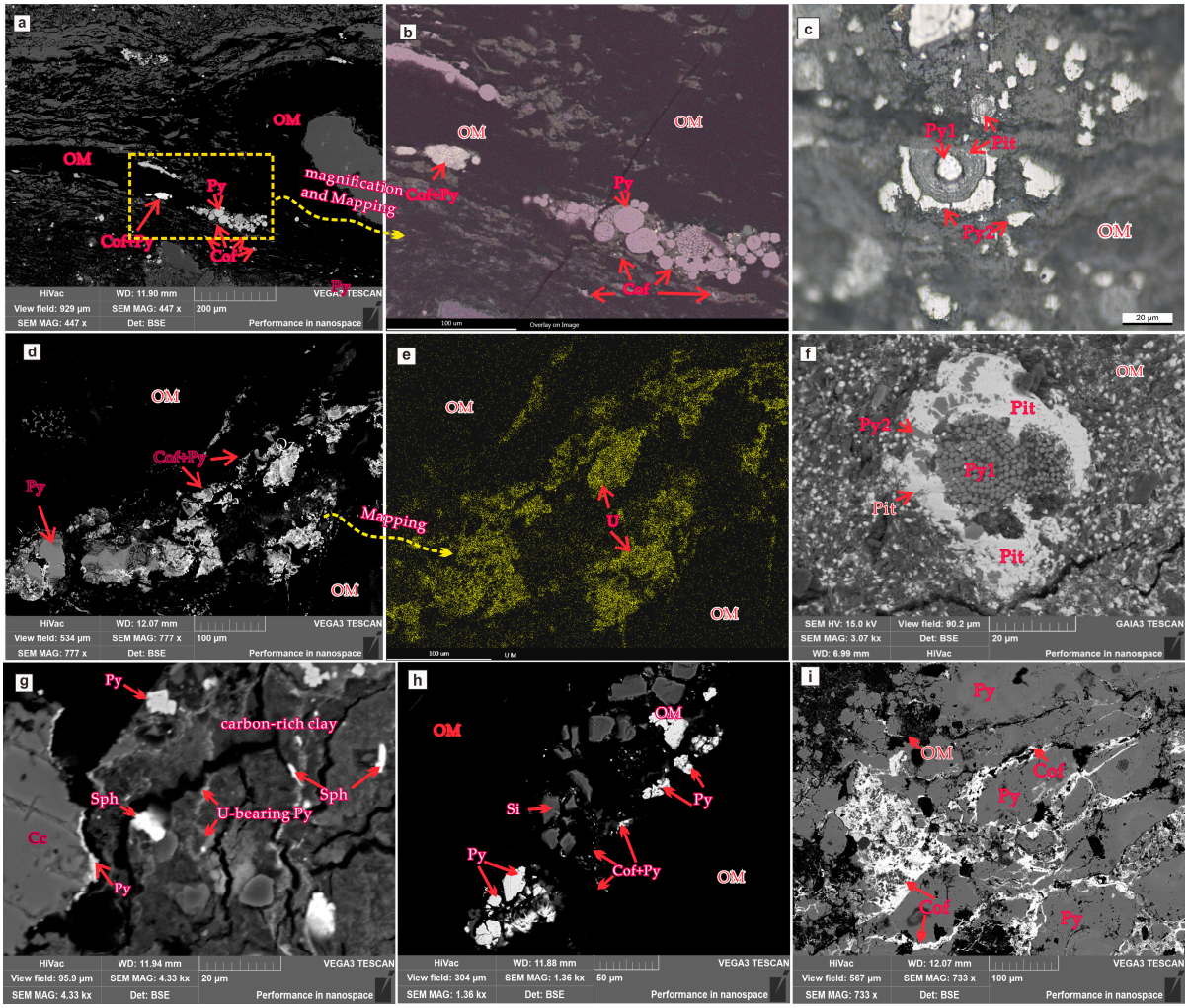


Figure 5. Images showing the distributions of the U minerals in the Louzhuangzi U deposit. Images (**b**,**e**) were captured via EDS; (**c**) is a reflected light image captured by a microscope; all others are

BSE images captured via SEM. (**a**–**e**) Coffinite in close symbiosis with pyrite in OM vein; (**f**) Coffinite and two stages of pyrite (Py1 and Py2) in bitumen; (**g**) Sphalerite symbiotic with pyrite containing cloudy-like U; (**h**) Tiny coffinite and pyrite particles symbiotic with silicon in bitumen; (**i**) Blocky coffinite in micropores and symbiotic with pyrite in sandstone. U = uranium; Pit = pitchblende; Cof = coffinite; Cc = calcite; Py = pyrite; Dol = dolomite; Sph = Sphalerite; Si = silicon.

The EPMA verified that the U minerals in the U-ores comprised mainly pitchblende and coffinite. The content of UO_2 represented between 57.5% and 86.4% (n = 22), and it was rich in S, Fe, P, Y, Ti, Zr, Nd, etc. The mapping images showed that Y, Th, Ti, Nd, and Zr were synchronously enriched (Figure 6).

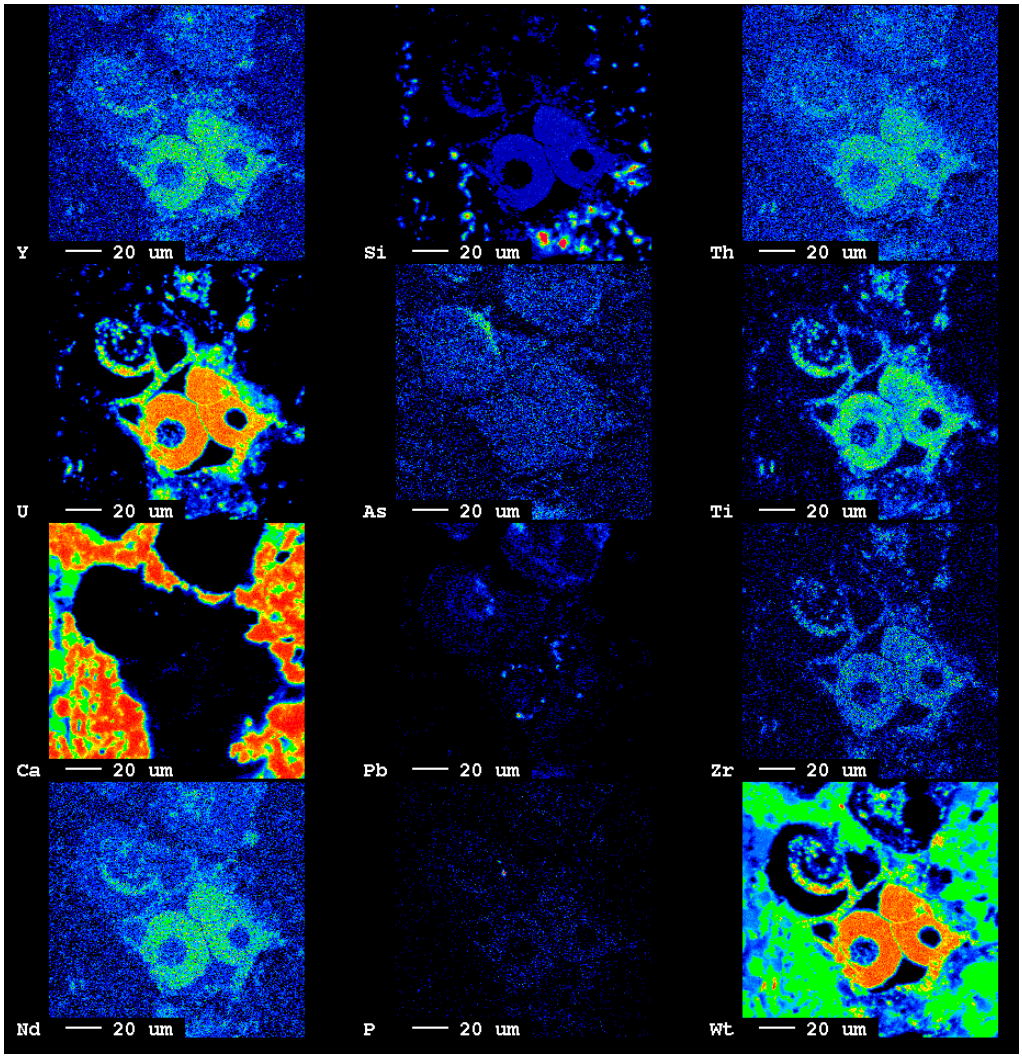


Figure 6. EPMA mapping images showing the distribution of different elements (Y, Si, Th, U, As, Ti, Ca, Pb, Zr, Nd, P) in the U-rich bitumen and a multi-element weight composition image (Wt).

4.2. Raman and Infrared Spectrum of the OM

The OM, closely related to U mineralization, was analyzed via Raman and infrared after microscopic observation. Fourteen sets of useful data were obtained. The analytical results are shown in Table 2. The Raman analysis showed that it had two obvious peaks near ~1370 cm^{-1} and ~1580 cm^{-1} (Table 2), with the Raman spectral characteristics of typical carbon materials (Figure 7a,b). The OM within the ore-bearing sandstone of the Toutunhe Fm exhibited a spectrum with peaks at 3395 cm^{-1}, 2926 cm^{-1}, 2869 cm^{-1}, 1695 cm^{-1}, 1598 cm^{-1}, 1438 cm^{-1}, 1375 cm^{-1}, 1220~1246 cm^{-1}, 1035~1043 cm^{-1}, and 753~853 cm^{-1} (Table 1, Figure 7c,d). The characteristic peaks observed in the infrared

spectra corresponded to specific molecular vibrations. For example, the peaks ranging from 3275 cm^{-1} to 3400 cm^{-1} indicated the stretching vibration of hydroxyl groups, while the peaks from 2925 cm^{-1} to 2960 cm^{-1} corresponded to the stretching vibration of the methyl and methylene groups in the aliphatic group. The corresponding functional groups of the OM within the Toutunhe Formation ore-bearing sandstone are detailed in Table 1. This composition differs from that of pyrobitumen, formed with a high degree of evolution and typical humic acid [4,34].

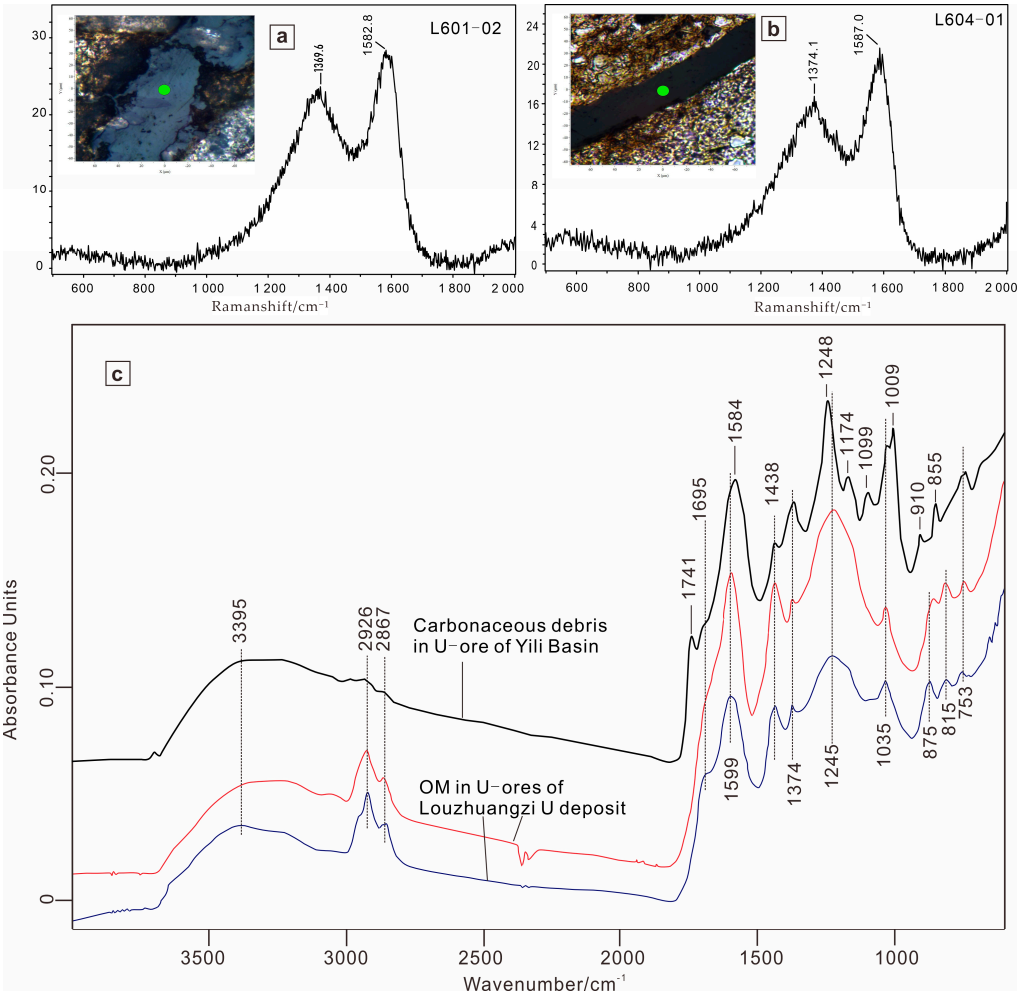


Figure 7. Raman (**a**,**b**) and infrared spectra (**c**) of the OM in U-ores at the Louzhuangzi U deposit, Junggar Basin, and the Honghaigou U deposit, Yili Basin.

Table 2. Raman shifts and infrared wavenumbers of the OM closely related to U mineralization at the Louzhuangzi U deposit.

Sample No.	Lithology	Test No.	Distribution	Raman Shift/cm^{-1}	Composition
L601-1	Dark gray coarse-grained sandstone	01	Fine-veined	1359.5, 1578.1	Carbon
		02	Fine-veined	1369.6, 1582.8	Carbon
L601-2		01	Veined	1377.6, 1582.8	Carbon
L601-6	Gray coarse-grained sandstone	01	Veined	1374.1, 1587.0	Carbon
		02	Veined	1372.3, 1581.5	Carbon
L602-4		01	Veined	1379.9, 1589.4	Carbon
		02	Veined	1362.7, 1590.4	Carbon
L604-1	Dark gray coarse-grained sandstone	03	Disseminated	1367.5, 1588.7	Carbon
		04	Disseminated	1369.4, 1589.6	Carbon

Table 2. *Cont.*

Sample No.	Lithology	Test No.	Distribution	IR Wavenumber/cm^{-1}	Interpretive Group
L601-6, L602-2, L602-4, L604-1	Dark gray, gray coarse-grained sandstone	01~05	Fine-veined, disseminated	3395 ± 2	–OH of water
				2926 ± 2	–CH_2 and –CH_3 of aliphatic
				2869 ± 1, 2856 ± 1	
				1695 ± 2	–C=O of carboxylic acid
				1598 ± 2	–C=C of aromatic
				1438 ± 2	Asymmetric vibration of CH_3 and CH_2
				1375 ± 1	Symmetric bending vibration of –CH_3
				1220~1240	–C=O stretching vibration and –OH deformation vibration of carboxylic acid
				1035~1043	C-O bending vibrations of alcohols and ethers
				867~875	–CH stretching vibrations of aromatic hydrocarbons
				815~818	
				753~757	

4.3. Trace Element Analysis

At the Louzhuangzi U deposit, 31 trace elements were determined from 16 U-symbiotic pyrites using in situ microregion methods, and 26 trace elements were determined from eight drill hole rock samples using the hole rock method. After the data comparison, it was found that there were 14 elements related to uranium mineralization (V, Cr, Co, Ni, Cu, Zn, Y, Mo, Cd, Re, As, Pb, Th), and their elemental content is listed in Table 3.

Table 3. Characteristic trace elements of pyrites and sandstone samples in U-ores from the Louzhuangzi U deposit. The unit of concentration is $\times 10^{-6}$.

Sample/Testing No.	Lithology	V	Cr	Co	Ni	Cu	Zn	Y	Mo	Cd	Re	As	Pb	Th	U
L601-5	U-mineralized sandstone	47.1	21.3	8.28	13.9	10.9	73	21.1	175	0.619	0.009		17.9	5.28	57.9
L602-2	U-mineralized sandstone	52.3	17.1	6.59	12.6	10.5	99	22.4	9.94	0.797	0.169		14.9	3.44	75
L604-4	U-mineralized sandstone	48.2	10.3	7.64	8.9	17.9	48.6	16.5	4.26	1.72	0.062		18.7	4.43	347
L604-5	U-mineralized sandstone	52.7	10.9	10	10.1	23.8	62.5	16.7	3.45	2.18	0.033		21.3	4.23	475
L604-6	U-mineralized sandstone	55.6	12.9	6.28	7.36	17.5	40	11.7	1.78	1.01	12.7		16.9	5.33	164
ZK1203-21	Gray coarse-grained sandstone with carbonaceous debris	45.3	25.4	4.73	7.42	5.39	36.4	16.3	15.5	0.188	1.34		13.6	6.65	22.4
ZK1203-25		49.1	24.5	5.32	10.2	11.6	32.1	14.5	1.14	0.068	0.136		12.4	5.1	1.83
ZK1302-50		25	14.4	5.16	7.93	4.92	24.1	12.8	0.364	0.05	0.002		13.9	5.22	1.06
ZK1302-56	Gray medium-grained sandstone	72.4	33.7	10.2	15.2	11.7	54.9	21.7	0.251	0.099	0.002		11.8	6.69	1.72
ZK1302-59	Gray coarse-grained sandstone with carbonaceous debris	45.5	24.4	9.08	13.1	11.1	47.5	21.6	0.744	0.103	0.335		13.4	5.99	1.47
L601-3-01	Pyrites in U-ore	14.1	1.1	52.5	271.6	117.7	3.4	64.2	569.5	0.0	/	440.8	112.2	0.68	12,567.5
L601-3-02	Pyrites in U-ore	10.6	0.0	127.5	385.2	89.7	3.8	40.6	832.0	0.3	/	470.8	130.3	0.44	7930.6
L601-3-03	Pyrites in U-ore	17.8	1.4	166.5	458.3	132.8	11.3	38.0	2353.6	0.5	/	915.1	174.8	0.65	9612.7
L601-5-01	Pyrites in U-ore	184.0	14.0	281.3	1243.5	600.3	52.4	458.8	10384.9	0.0	/	1688.0	894.7	9.42	123,975.0
L601-5-02	Pyrites in U-ore	1.2	3.5	45.6	184.5	86.8	5.5	0.6	237.0	0.6	/	317.4	29.9	0.05	53.2
L601-6-01	Pyrites in U-ore	5.0	0.3	21.7	110.3	64.1	10.0	6.7	172.3	0.2	/	385.4	19.9	0.11	682.8
L601-6-02	Pyrites in U-ore	9.2	0.0	87.6	270.7	70.0	4.0	5.4	1550.2	0.3	/	922.3	66.4	0.05	350.1
L602-2-01	Pyrites in U-ore	19.7	4.2	1471.6	3185.6	315.8	8.3	13.3	2926.9	0.5	/	2083.5	592.5	0.41	1680.3
L602-2-02	Pyrites in U-ore	8.2	2.4	199.4	553.4	104.9	3.4	89.0	1583.3	0.0	/	528.4	97.3	0.29	2767.6
L602-4-01	Pyrites in U-ore	26.2	4.4	645.6	1383.1	152.1	6.3	7.1	2438.4	0.6	/	951.6	232.6	0.40	1265.5
L602-4-02	Pyrites in U-ore	50.0	1.7	328.4	833.2	116.4	3.4	1711.7	3798.8	1.2	/	582.2	139.4	0.41	22,406.9
L602-4-03	Pyrites in U-ore	11.2	0.0	92.9	302.7	90.4	3.3	8.7	1143.7	0.3	/	435.5	35.3	0.18	3323.7
L604-4-01	Pyrites in U-ore	20.5	2.7	251.8	598.1	103.9	9.9	3.1	2625.1	0.0	/	438.7	135.6	0.23	154.7
L604-4-02	Pyrites in U-ore	10.7	0.8	208.6	623.5	97.4	5.1	25.2	2173.0	0.3	/	512.3	93.9	0.25	343.6
L604-5-01	Pyrites in U-ore	10.3	3.3	14.7	17.5	6.8	2403.4	14.3	40.6	21.3	/	5924.3	4.1	0.09	761.2
L604-5-01	Pyrites in U-ore	9.8	5.1	19.2	19.4	27.4	1697.3	17.3	120.1	36.0	/	4054.3	11.2	0.11	1322.0

4.3.1. Trace Elements Analyzed via the Hole Rock Method

The content of the characteristic elements was very low in the primary barren sandstone of the Toutunhe Formation (Table 3). Compared with the CLARKE value (crustal abundance), the barren sandstone was characterized by the loss of V, Cr, Co, Ni, Cu, Zn, etc. Meanwhile, the content of U, Th, Pb, and Y was similar to their CLARKE values; Re had a certain degree of enrichment in the coal-bearing sandstone, and the enrichment ratio reached 5~387 times its CLARKE value. However, the content of U, Re, and Mo in the U-ores was generally high and often more than 100 times their CLARKE values (the maximum values of U and Mo were 344 and 269 times their CLARKE values, respectively). In some cases, it was more than 1000 times their CLARKE values (the maximum of Re was up to 31,751 times its CLARKE value). This was especially pronounced in the rich U-ores (Figure 8), and elements such as Cd, Cu, Zn, and Y were also enriched to a certain extent, as their values were generally more than twice as high as those in the barren sandstone. This enrichment is consistent with the abundance of metal sulfur observed in the U-ores, which are rich in pyrite and sphalerite, as observed via SEM.

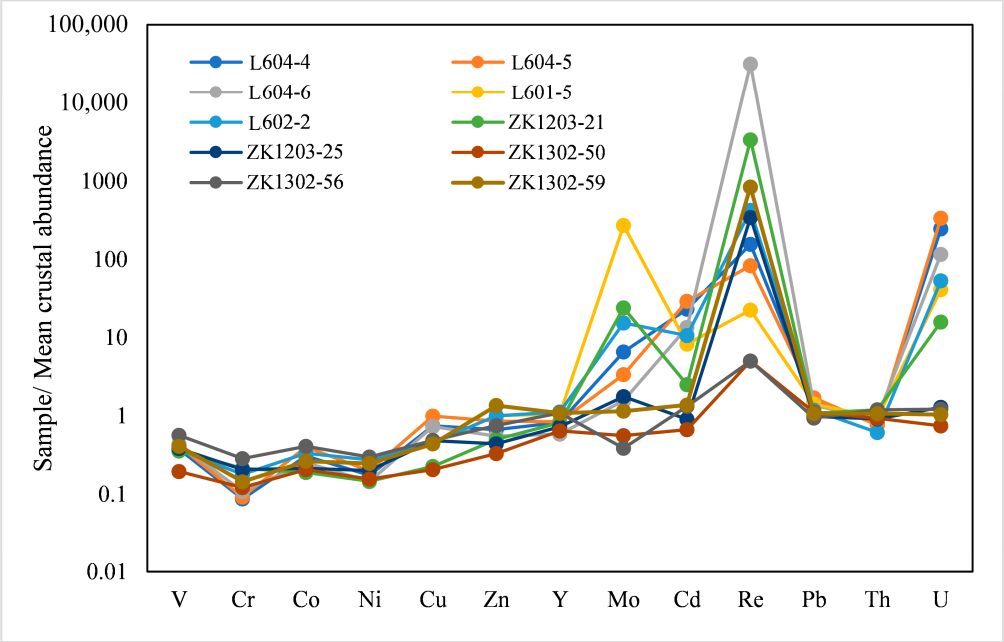


Figure 8. Characteristic trace element change curves of U-ores and primary barren gray sandstone of Toutunhe Fm in the Louzhuangzi U deposit.

4.3.2. Trace Elements of U-Symbiotic Pyrite Analyzed via La-ICPMS

The content of U, Mo, and As in the pyrite of the U-ores was generally high, often more than 100 times their CLARKE values and, in some cases, even more than 1000 times their CLARKE values. Additionally, Pb, Co, Ni, Cu, and Y were enriched to a certain extent, with most reaching more than 10 times their CLARKE values. Zn was also enriched in some specific samples, reaching more than 10,100 times its CLARKE value. Generally, U had a good correlation with Mo, Pb, and Cu, and their correlation coefficients were 0.6245, 0.488, and 0.4831, respectively. The distribution curves of U and Mo, Pb, and Cu in the pyrites of the U-ore showed consistent trends (Figure 9), indicating that the more intense the U mineralization, the more concentrated the U, Mo, Pb, and Cu content. The correlation between Y, Ni, Zn, and U was not obvious. Their correlation coefficients were 0.1486, 0.0353, and 0.014, respectively (Figure 9). However, relative to their CLARKE values, they were still significantly enriched. In particular, Zn was strongly enriched in two samples, up to more than 1600×10^{-6}. The results for these elements indicated that the enrichment of Fe, Cu, Mo, and Zn occurred simultaneously during the enrichment of uranium.

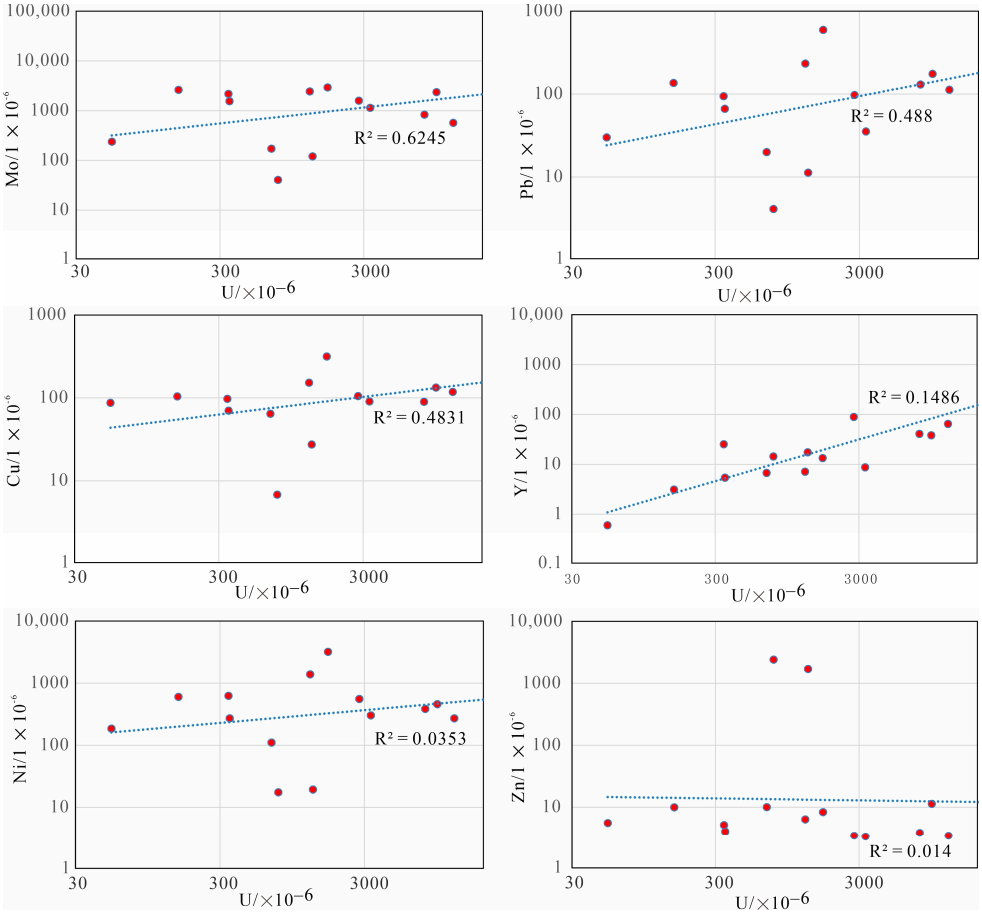


Figure 9. Diagrams representing the relationship between typical trace elements (Mo, Pb, Cu, Y, Ni, Zn) and the U content.

4.4. Carbon Isotope of OM

The carbon isotope values of the OM in the U-ores and the barren sandstone samples from the primary zone of the Louzhuangzi U deposit are shown in Table 4. The variation in the C isotope values of the OM in the U-ore ranged from −26.9‰ to −22.2‰ (the samples from drill holes L601 and L604, with a mean of −23.8‰, N = 10) [35]. Meanwhile, the range of the C isotope values of the OM in the barren sandstone samples of the primary zone was between −25.6‰ and −22.8‰ (mean of −24.1‰, N = 8) [36]. The C isotope values of the OM in the U-ores and barren sandstone of the primary zone were generally similar. They fell within the C isotope range of humic-type coal (the C isotope of humic coal is always between −25.5‰ and −23.5‰) [35]. They were significantly different from those of sapropelic coal (the C isotope of sapropelic coal is always between −35‰ and −30‰) [36] and typical crude oil in the Jurassic formation of the southern Junggar Basin, as reported by previous scholars (concentrations between −28‰ and −26‰) [36,37].

Table 4. $\delta^{13}C$ isotope compositions of the OM in U-ores and barren sandstone samples of the primary zone from the Louzhuangzi U deposit.

Sample No.	Lithology	$^{13}C_{V\text{-}PDB}$/‰	Sample No.	Lithology	$^{13}C_{V\text{-}PDB}$/‰
L601-1	Dark gray coarse-grained sandstone	−24.2	L604-6	Dark gray coarse-grained sandstone	−23.8
L601-2	Dark gray coarse-grained sandstone	−23.0	ZK1203-21	Gray coarse-grained sandstone with carbonaceous debris	−23.4

Table 4. *Cont.*

Sample No.	Lithology	$^{13}C_{V\text{-}PDB}$/‰	Sample No.	Lithology	$^{13}C_{V\text{-}PDB}$/‰
L601-4	Gray-white coarse-grained sandstone	−26.9	ZK1203-24	Coal	−23.6
L601-6	Gray coarse-grained sandstone	−23.4	ZK1302-10	Coal	−25.3
L604-1	Dark gray coarse-grained sandstone	−24.7	ZK1302-40	Gray coarse-grained carbonaceous sandstone	−24.6
L604-2	Dark gray coarse-grained sandstone	−23.1	ZK1302-50		−25.6
L604-3	Gray coarse-grained sandstone	−24.3	ZK1302-54	Gray coarse-grained coal-bearing sandstone	−22.8
L604-4	Gray coarse-grained sandstone	−22.2	ZK1302-57		−23.9
L604-5	Gray coarse-grained sandstone	−22.8	ZK1302-60		−23.4

4.5. Sulfur Isotope of U-Symbiotic Pyrite

The sulfur isotope data of the U-symbiotic pyrite in the U-ores from the Louzhuangzi U deposit are shown in Table 5. The $\delta^{34}S$ values of the U-symbiotic pyrites varied between −42.6‰ and 37.2‰ (mean of 2.7‰, N = 28). Their variation covered a broad range, and their $\delta^{34}S$ values exhibited typical sedimentary genesis characteristics [38], which means that they differed greatly from those of magmatic and metamorphic origin [39]. Moreover, most of the S isotope values overlapped with those of coal and crude oil [35] (Figure 10). A small number of S isotopes had negative values, which may be related to the bacterial reduction of sulfates (BSR).

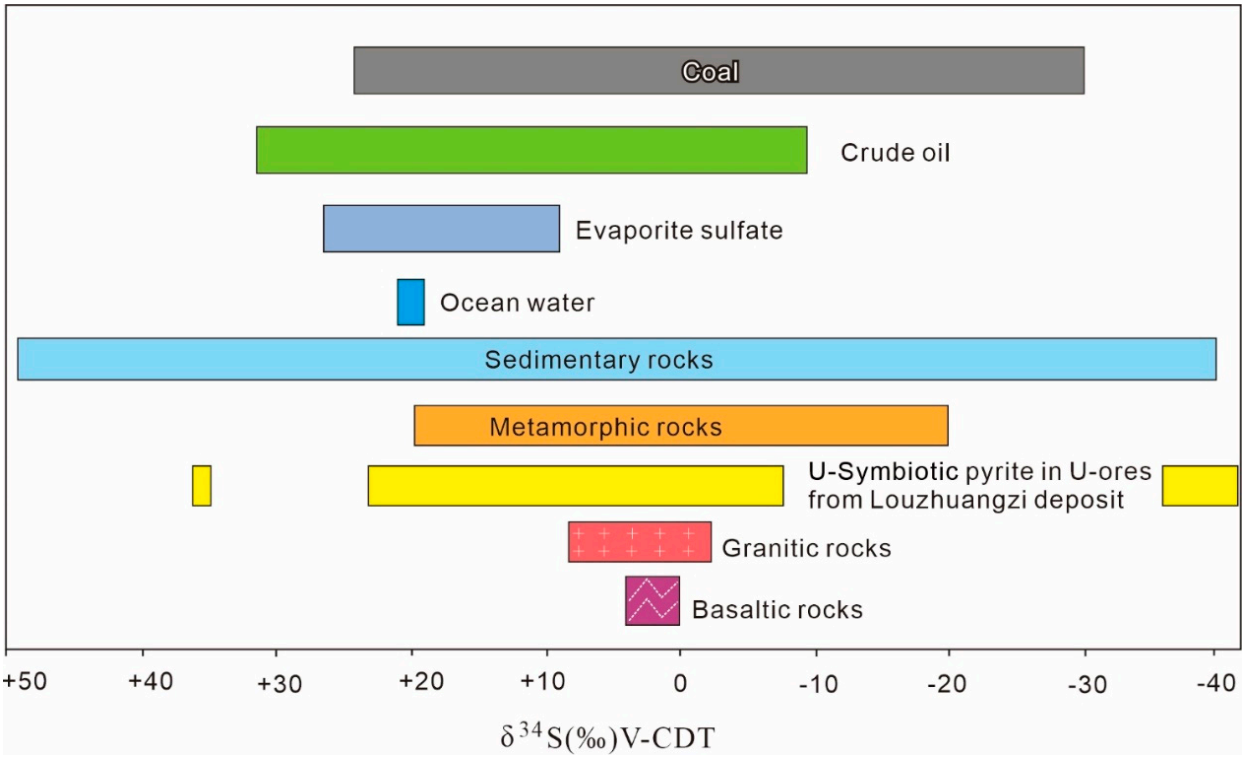


Figure 10. Sulfur isotope distribution of U-symbiotic pyrite from the Louzhuangzi U deposit and typical rock and energy resources (modified from references [35,38,39]).

Table 5. $\delta^{34}S$ isotope compositions of U-symbiotic pyrite in U-ores from the Louzhuangzi U deposit.

Sample No.	Lithology	$\delta^{34}S_{V\text{-}CTD}$ (‰)	Sample No.		$\delta^{34}S_{V\text{-}CTD}$ (‰)
L602-1-1	Dark gray coarse-grained sandstone (U-ore)	−2.13	L604-2-1	Dark gray coarse-grained sandstone (U-ore)	11.73
L602-1-3		−0.79	L604-2-2		6.78
L602-1-4		−4.80	L604-2-3		37.20
L602-1-5		−42.63	L604-2-5		23.18
L602-1-7		3.71	L601-5-1	Gray coarse-grained sandstone (U-ore)	−40.51
L602-1-8		3.56	L601-5-2		0.90
L602-3-1	Gray coarse-grained sandstone (U-ore)	11.74	L601-5-3		4.60
L602-3-3		3.73	L604-4-1	Gray coarse-grained sandstone (U-ore)	16.34
L602-3-4		12.40	L604-4-2		−7.77
L602-3-6		−36.52	L604-4-3		9.45
L604-1-1	Dark gray coarse-grained sandstone (U-ore)	−4.22	L604-5-1	Gray coarse-grained sandstone (U-ore)	−3.56
L604-1-4		3.19	L604-5-2		10.48
L604-1-6		23.58	L604-5-3		11.01
L604-1-8		22.75	L604-5-4		2.64

5. Discussion

5.1. Nature and Sources

OM (humic acid, bitumen, carbonaceous) contributes significantly to the U mineralization of sandstone-hosted U deposits. Therefore, understanding the nature and sources of OM is important in clarifying the metallogenic mechanism. The observation results for the drilling core showed that there are two types of OM at the Louzhuangzi U deposit. The OM in the U-ores is mainly distributed in the form of fine veins (some OM is vertical with the strata) and disseminated in the fracture zones or pores of the sandstone. The OM in the barren sandstone is scattered with carbonaceous debris, which is inherited from the sedimentary process. Microscopically, the OM in the U-ores presents a flowing structure, showing its mobility characteristics. The laser Raman analysis showed that the OM displayed two characteristic peaks near 1370 cm^{-1} and 1580 cm^{-1}, which are characteristic of typical carbonaceous substances [23,40,41]. Stable isotope studies have shown that the $\delta^{13}C$ value of the OM in U-ore is −26.9‰ to −22.2‰ (mean of −23.8‰), and the C isotope value of the OM in barren sandstone is comparable to that of humic-type coal [35]. However, it is very different from that of sapropelic coal and typical crude oil [35]. The infrared spectrum analysis showed that the OM in the U-ores has complex functional groups, and its main composition is comparable to that of the carbonaceous debris in the U-ores of the Toutunhe Fm at the Honghaigou U deposit, Yili Basin, Xinjiang Province. Meanwhile, it is different from the pyrobitumen formed with a high degree of evolution [4] and typical humic acid. The sulfur isotopic values of U-symbiotic pyrite varied between −42.6‰ and 37.2‰ (mean of 2.7‰, N = 28). Most of the S isotopic values overlapped with those of coal and crude oil [35], and a small number of S isotopes had negative values, which may be related to typical bacterial sulfate reduction (BSR) [23,42,43]. The above results suggest that the OM in the U-ores of the Louzhuangzi U deposit is likely bitumen formed by the cracking–differentiation of coal-derived hydrocarbons, with obvious migration characteristics. Some oil production test holes have been investigated approximately 3 km southwest of the Louzhuangzi U deposit. Based on the form of OM in the drill cores, the microscopic features, the C isotope values, and the S isotope of the U-symbiotic pyrite at the Louzhuangzi U deposit, it was concluded that the OM is related to the evolution of the coal-bearing strata, such as the Toutunhe Fm and Xishanyao Fm.

5.2. Relationship between OM and U Mineralization

OM plays a pivotal role in U mineralization, encompassing coordination, reduction, and adsorption [42]. In this study, the presence of bitumen or humus within the U-ores suggested their formation through the cracking and differentiation of coal-derived hydrocarbons. However, the specific role of coal-derived hydrocarbons in the U mineralization process remains to be elucidated.

Previous researchers have posited two primary functions of hydrocarbon fluids in U mineralization: they serve to reduce the U- and oxygen-containing fluids; and they facilitate the transport of minerals and hydrocarbon fluids during migration [41,42]. The ore body characteristics of the Louzhuangzi U deposit include several significant aspects: (1) its strict control by the gray-white alteration zone (this is related to kaolinization alteration), with darker central areas of U mineralization; (2) the tabular and banded extension of the ore bodies; and (3) the dominance of OM and sulfide in the center of the surrounding U-mineralized rock, with higher-grade U-ores often found in areas rich in OM. Consequently, it is evident that the output of the ore body is tightly regulated by the gray-white alteration zone and the presence of black OM.

The scanning electron microscopy investigations revealed the common occurrence of pitchblende and coffinite alongside metal sulfides (pyrite, sphalerite) in the OM. The quantitative analysis of the trace elements in the drill rocks and U-symbiotic pyrite indicated the enrichment of U, Mo, Re, Y, Cu, Zn, and other elements during U mineralization. Although the uranium content in the barren sandstone of the primary zone was generally low (U content < 2.0×10^{-6}), it significantly increased in the gray-white alteration zone (U content $\approx 14.0 \times 10^{-6}$), particularly in bitumen-rich zones (U-content $\approx 238 \times 10^{-6}$). This suggested the possibility of two processes of uranium enrichment, where the formation of a U-rich ore may be linked to the activity of hydrocarbon fluids, particularly within the bitumen matrix.

5.3. Metallogenic Processes and Genesis of Louzhuangzi U Deposit

The interlayer oxidation-zone-type uranium deposit represents a conventional metallogenic model that is widely utilized in the exploration of uranium resources in Central Asian countries. This model suggests the transportation of U by oxidizing groundwater within permeable layers down to the redox zone [19–21]. However, this model fails to account for the ubiquitous presence of bitumen in the U mineralization of the Louzhuangzi U deposit. An alternative metallogenic model for sandstone-hosted U deposits proposes the involvement of organic-rich fluids derived from the evolution of deep source rocks, which coordinate or chelate with ore-forming materials to facilitate the migration of U together with organic-rich fluids. Some scholars have also reported examples of uranium deposits formed by the cracking of hydrocarbon fluids containing uranium, such as the U deposit of the Franceville Basin in Gabon [24] and the Witwatersrand gold–uranium deposit in Africa [44]. The functional groups within the OM, including aliphatic, aromatic, carboxyl, hydroxyl, and carbonyl groups, play a significant role in the U mineralization process, as exemplified by deposits such as the Hadatu deposit in the Erlian Basin [5].

Our studies indicated that the formation of a U-rich ore may be associated with the activity of hydrocarbon fluids within the bitumen matrix, which could have evolved from coal-bearing strata. While three sets of coal-bearing strata exist in the Jurassic of the southern Junggar Basin, including the Toutunhe Fm, Xishanyao Fm, and Badaowan Fm, their low U content (<3×10^{-6}) suggested that it is unlikely that the U is solely derived from these strata. Additionally, the original sedimentary environment of the third rhythmic layer in the Toutunhe Fm lacks the oxidation conditions required for exudation and U mineralization. Previous studies have identified the main U mineralization age of the Louzhuangzi U deposit to be around 53 ± 5 Ma [21], coinciding with large-scale uplift in the southern Junggar Basin during this period. Consequently, at least two stages of U mineralization overlap at the Louzhuangzi U deposit (Figure 11).

Consistent with the U mineralization in the gray rock series, the classical theory of U mineralization in the interlayer oxide zone is accepted by the majority of scholars throughout the world. Therefore, the first stage of U mineralization may be consistent with the interlayer oxidation-zone-type uranium mineralization model. However, the second U mineralization event is difficult to explain via the interlayer oxidation-zone-type uranium mineralization model. Thus, this study suggested that the first stage (Figure 11a) may have been primarily controlled by interlayer oxidation fluids, where U-bearing and oxygen-rich water infiltrated the oxidized sandstones of the Toutunhe Fm, precipitating U through reduction processes. The second stage (Figure 11b) may have been predominantly controlled by the exudation of hydrocarbon fluids from coal-bearing strata, which not only carried uranium into oxidized sandstones but also acted as reducing agents, resulting in secondary enrichment and U mineralization. Simultaneously, these hydrocarbon fluids underwent cracking into bitumen and light hydrocarbons, while the oxidized formations were reduced to gray-white compounds.

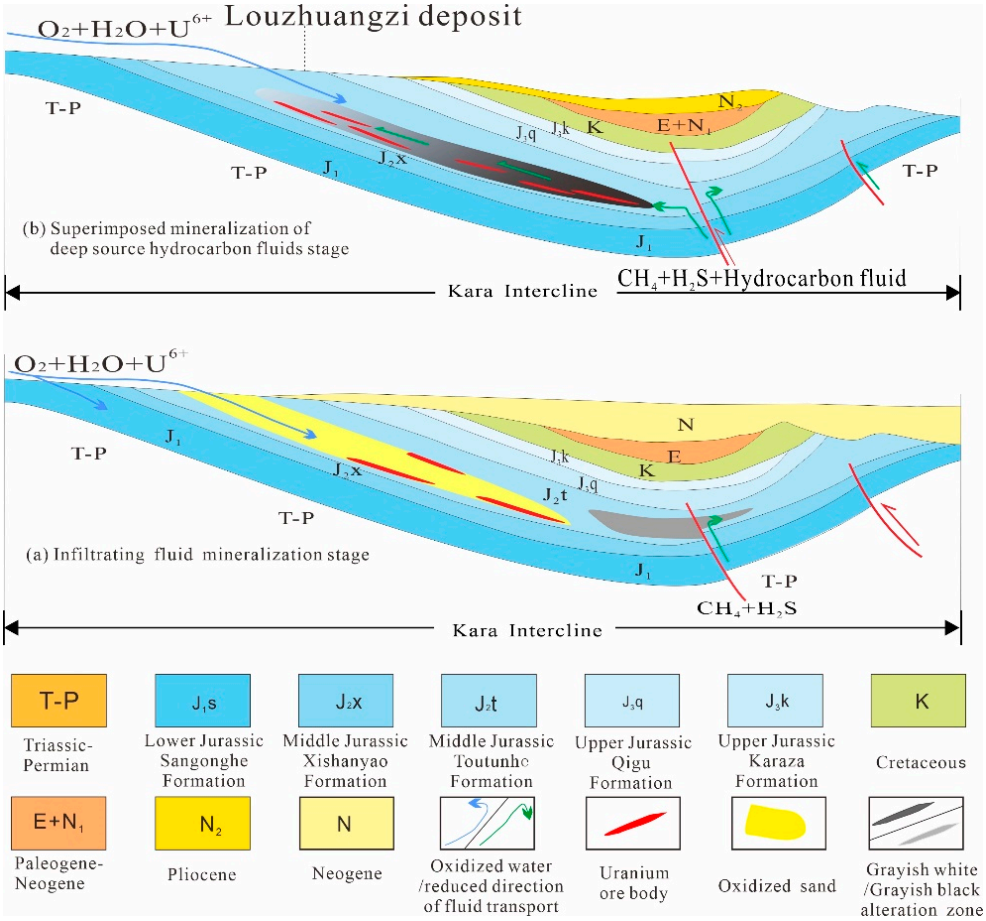


Figure 11. A conceptual model of the U mineralization and metallogenic process of the Louzhuangzi U deposit. (**a**) The gray sandstone containing carbonaceous debris was formed via sedimentation, and the first stage of U mineralization at the Louzhuangzi U deposit was formed via the interlayer oxidation of supergene fluids, and then the formation was oxidized to a brown or light yellow color. (**b**) The second stage of U mineralization at the Louzhuangzi U deposit occurred during the cracking of hydrocarbon-containing fluids in oxidized formations, and the hydrocarbon-containing fluids evolved from the coal-bearing strata in the lower part of the Toutunhe Formation. The strata were also reduced to gray or grayish-white compounds.

6. Conclusions

Our studies characterized the types of organic matter (OM) present in the U-ores of the Louzhuangzi U deposit in the southern Junggar Basin, China, providing direct evidence of the involvement of mobile hydrocarbon fluids in U mineralization. We proposed a two-stage U mineralization model for the formation of the Louzhuangzi U deposit. In the first stage, U mineralization was likely primarily controlled by interlayer oxidation fluids, where U was transported to carbonaceous sandstones and precipitated through reduction processes. In the second stage, U mineralization may have been predominantly controlled by the exudation of hydrocarbon fluids from coal-bearing strata, potentially migrating together with hydrocarbon fluids originating from the lower strata, such as the Xishanyao Fm. In summary, our research confirmed the involvement of hydrocarbon fluids in the U mineralization process at the Louzhuangzi U deposit of the southern Junggar Basin, China.

Author Contributions: Conceptualization, B.-Q.H. and Z.-B.H.; data curation, Z.-B.H., L.-F.Q. and Y.W.; formal analysis, B.-Q.H. and Z.-B.H.; investigation, Z.-B.H. and M.-H.Z.; methodology, L.-F.Q. and Z.-B.H.; project administration, H.C. and Y.-F.L.; resources, B.-Q.H., Y.W., L.-F.Q., H.C., W.-W.J. and H.-L.J.; writing—original draft, Z.-B.H.; writing—review and editing, B.-Q.H. and Z.-B.H. All authors have read and agreed to the published version of the manuscript.

Funding: This research was funded by the "Assume Leadership" project of the Natural Uranium Industry Technology Innovation Consortium, "Key factors and metallogenic mechanism of red uranium formation in the northern sedimentary basin", No. 202301.

Data Availability Statement: The original contributions presented in the study are included in the article, further inquiries can be directed to the corresponding author/s.

Acknowledgments: We are highly grateful to the No. 216 Nuclear Geological Brigade, China National Nuclear Corporation (CNNC), for the fieldwork investigations in the study area. Our thanks are also given to the editors and reviewers for the constructive comments that helped to improve the paper.

Conflicts of Interest: The authors declare no conflicts of interest.

References

1. Zhang, J.D. Innovation and development of metallogenic theory for sandstone type uranium deposit in China. *Uranium Geol.* **2016**, *32*, 321–332. (In Chinese with English abstract)
2. International Atomic Energy Agency (IAEA). *World Uranium Geology, Exploration, Resources and Production*; IAEA Library: Vienna, Austria, 2020.
3. Jiao, Y.Q.; Wu, L.Q.; Rong, H.; Zhang, F. Review of basin uranium resources in China. *Earth Sci.* **2021**, *46*, 2675–2696. (In Chinese with English abstract)
4. Qiu, L.F.; Li, X.D.; Liu, W.S.; Hu, B.Q.; Gao, L.; He, Z.B. Uranium deposits of Erlian Basin (China): Role of carbonaceous debris organic matter and hydrocarbon fluids on uranium mineralization. *Minerals* **2021**, *11*, 532. [CrossRef]
5. Li, Z.Y.; Liu, W.S.; Li, W.T.; Li, X.D.; Qin, M.K.; Cai, Y.Q.; Zhang, Y.L.; He, S.; Wu, Q.B.; Qiu, L.F.; et al. Exudative metallogeny of the Hadatu sandstone-type uranium deposit in the Erlian Basin, Inner Mongolia. *Geol. China* **2022**, *49*, 1009–1047. (In Chinese with English abstract)
6. Ren, Y.S.; Yang, X.Y.; Hu, X.W.; Wei, J.L.; Tang, C. Mineralogical and geochemical evidence for biogenic uranium mineralization in Northern Songliao Basin, NE China. *Ore Geol. Rev.* **2021**, *141*, 104556. [CrossRef]
7. Wang, G.; Wang, G.R.; Lu, K.G.; Tang, X.F. Review on the Uranium geology efforts and outlook for future exploration in Junggar Basin. *Uranium Geol.* **2016**, *32*, 340–349. (In Chinese with English abstract)
8. He, Z.B.; Qin, M.K.; Song, J.Y.; Guo, Q.; Xu, Q.; Liu, Z.; Yang, Y.; Huang, S. A study of metallogenic environments and prospecting direction of Jurassic sandstone-type uranium deposit in northeastern Junggar Basin. *Miner. Depos.* **2018**, *37*, 175–190. (In Chinese with English abstract)
9. Huang, S.H.; Qin, M.K.; Xu, Q.; He, Z.B.; Liu, Z.Y.; Selby, D. Supermposed uranium metallogenesis between deep hydrocarbon fluid and supergene oxidation fluid in the Northwestern margin of Junggar Basin. *Acta Geol. Sin.* **2018**, *92*, 1493–1506. (In Chinese with English abstract)
10. Qin, M.K.; He, Z.B.; Liu, Z.Y.; Guo, Q.; Song, J.Y.; Xu, Q. Study on metallogenic environments and prospective direction of sandstone type uranium deposits in Junggar Basin. *Geol. Rev.* **2017**, *63*, 1255–1269. (In Chinese with English abstract)
11. Qin, M.K.; Huang, S.H.; He, Z.B.; Xu, Q.; Song, J.Y.; Liu, Z.; Guo, Q. Evolution of tectonic uplift, hydrocarbon migration, and uranium mineralization in the NW Junggar Basin: An apatite fission-track thermochronology study. *Acta Geol. Sin.—Engl. Ed.* **2018**, *92*, 1901–1916. [CrossRef]

12. Chen, Z.; Liu, J.; Gong, H.; Han, F.; Briggs, S.M.; Zheng, E.; Wang, G. Late Cenozoic tectonic activity and its significance in the Northern Junggar Basin, Northwestern China. *Tectonophysics* **2011**, *497*, 45–56. [CrossRef]
13. Wu, Z.J.; Han, X.Z.; Ji, H.; Cai, Y.F.; Xue, L.; Sun, S.J. Mesozoic-Cenozoic tectonic events of eastern Junggar Basin, NW China and their significance for uranium mineralization: Insights from seismic profiling and AFT dating analysis. *Ore Geol. Rev.* **2021**, *139*, 104488. [CrossRef]
14. Hu, X.W.; Yang, X.Y.; Wu, Z.J.; Ren, Y.S.; Miao, P.S. Sedimentological, petrological, and geochemical constraints on the formation of the Beisantai sandstone-type uranium deposit, Junggar Basin, NW China. *Ore Geol. Rev.* **2022**, *141*, 104668. [CrossRef]
15. Zhou, Y.; Liu, Z.L.; Kaarel, M.; Li, F.J.; Peng, N.; Kuang, H.W.; Liu, Y.Q.; Liu, Y.X.; Zhang, M.H. Geochemical characteristics of Jurassic sandstones on the southern margin of the Junggar Basin: Constraints on provenance and sandstone-type uranium mineralization. *Ore Geol. Rev.* **2022**, *146*, 104922. [CrossRef]
16. Zhang, P.F.; Li, F.J.; Liu, Z.L.; Liu, Y.X.; Ma, X.K.; Liu, B. Detrital zircon U–Pb geochronology and Hf isotopes of Mesozoic through Cenozoic sandstones from the southern Junggar Basin, NW China: Implications for the provenances and uranium source. *Geol. J.* **2022**, *57*, 3829–3850. [CrossRef]
17. Hu, X.W.; Yang, X.Y.; Ren, Y.S.; Du, G.F.; Wu, Z.J. Genesis of interlayer oxidation zone-type uranium deposit in the channel conglomerates, Beisantai area, Junggar Basin: An insight into uranium mineralization. *Ore Geol. Rev.* **2022**, *140*, 104557. [CrossRef]
18. Huang, S.H.; Qin, M.K.; Liu, Z.Y.; Xu, Q.; Guo, Q. Impact of diagenesis and hydrocarbon charging on sandstone uranium mineralization: An example of Toutunhe Formation in Liuhuanggou area, southern Junggar Basin. *Acta Sedimentol. Sin.* **2016**, *34*, 250–259. (In Chinese with English abstract)
19. Huang, S.; Jia, W.W.; Yan, J.J. Discussion on the relationship between sand body characteristics and uranium mineralization in the lower member of Toutunhe formation in Louzhuangzi area, southern margin of Junggar Basin. *Uranium Geol.* **2023**, *39*, 522–532. (In Chinese with English abstract)
20. Jia, W.W.; Wang, G.R.; Tang, X.F.; Huang, S.; Yan, J.J. Discussion on the relationship of different types of alteration zones to the uranium mineralization in Toutunhe formation of Louzhuangzi area, Southern Margin of Junggar Basin. *World Nucl. Geosci.* **2023**, *40*, 152–161. (In Chinese with English abstract)
21. Lu, K.G.; Du, M.; Sun, X.; Jia, W.W.; Wang, S.Y. Metallogenic Controlling Factors and Genetic Analysis of Sandstone Uranium Deposit in the Lower Member of Toutunhe Formation in Louzhuangzi Area, Southern Junggar Basin. *Uranium Geol.* **2023**, *39*, 507–521. (In Chinese with English abstract)
22. Bonnettia, C.; Zhou, L.L.; Rieglerc, T.; Bruggerd, J.; Fairclough, M. Large S isotope and trace element fractionations in pyrite of uranium roll front systems result from internally-driven biogeochemical cycle. *Geochim. Cosmochim. Acta* **2020**, *282*, 113–132. [CrossRef]
23. Goldhaber, M.B.; Hemingway, B.S.; Mohagheghi, A.; Reynolds, R.L.; Northrop, H.R. Origin of coffinite in sedimentary rocks by a sequential adsorption-reduction mechanism. *Bull. Minéralogie* **1987**, *110*, 131–144. [CrossRef]
24. Lecomte, A.; Michels, R.; Cathelineau, M.; Morlot, C.; Brouand, M.; Flotte, N. Uranium deposits of Franceville basin (Gabon): Role of organic matter and oil cracking on uranium mineralization. *Ore Geol. Rev.* **2020**, *123*, 103579. [CrossRef]
25. Landais, P. Organic geochemistry of sedimentary uranium ore deposits. *Ore Geol. Rev.* **1996**, *11*, 33–51. [CrossRef]
26. Qiu, L.F.; Wu, Y.; Wang, Q.; Wu, L.F.; He, Z.B.; Peng, S.; Fan, Y.F. Metallogenic mechanism of typical carbonate-hosted uranium deposits in Guizhou (China). *Minerals* **2022**, *12*, 585. [CrossRef]
27. Qiu, L.F.; Li, Z.Y.; Zhang, Z.L.; Wang, L.H.; Li, Z.C.; Han, M.Z.; Wang, T.T. Characteristics of organic matter in Lower Cretaceous ore-bearing sandstones and its relationship with uranium mineralization in the northern Ordos Basin. *Earth Sci. Front.* **2024**, 1–20. (In Chinese with English abstract) [CrossRef]
28. Xiao, W.J.; Windley, B.F.; Huang, B.C.; Han, C.M.; Yuan, C.; Chen, H.L.; Sun, M.; Sun, S.; Li, L.J. End-Permian to mid-Triassic termination of the accretionary processes of the southern Altaids: Implications for the geodynamic evolution, Phanerozoic continental growth and metallogeny of Central Asia. *Int. J. Earth Sci.* **2009**, *98*, 1189–1217. [CrossRef]
29. He, D.F.; Zhang, L.; Wu, S.T.; Li, D.; Zhen, Y. Tectonic evolution stages and features of the Junggar Basin. *Oil Gas Geol.* **2018**, *39*, 845–860. (In Chinese with English abstract)
30. Chen, S.P.; Qi, J.F.; Yu, F.S.; Yang, Q. Deformati on Characteristics in the Southern Margin of the Junggar Basin and Their Controlling Factors. *Acta Geol. Sin.* **2007**, *81*, 151–157.
31. Liu, H.F.; Liang, H.S.; Cai, L.G.; Xia, Y.P.; Liu, L.Q. Tectonic styles and foreland basin evolution of foreland thrusts on both sides of Tianshan mountains. *Earth Sci.* **1994**, *6*, 727–741. (In Chinese with English abstract)
32. Avouac, J.P.; Tapponnier, P.; Bai, M.; You, H.; Wang, G. Active thrusting and folding along the northern Tien Shan and Late Cenozoic rotation of the Tarim relative to Dzungaria and Kazakhstan. *J. Geophys. Res. Solid. Earth* **1993**, *98*, 6755–6804. [CrossRef]
33. Qiu, L.F.; Li, Z.Y.; He, F.; Wu, Z.Q.; Liu, K.P.; Mao, N.; Li, M.H. Characteristics of organic matter in lower Cretaceous ore-bearing sandstone and its relationship with uranium mineralization in Southwest of Ordos Basin. *Uranium Geol.* **2024**, *40*, 41–56. (In Chinese with English abstract)
34. Song, H.Y.; Yin, Y.; Song, J.Z. Study on the Chemical Composition and structure of humic acids from different sources. *J. South China Norm. Univ. (Nat. Sci. Ed.)* **2009**, *123*, 61–66. (In Chinese with English abstract)
35. Zheng, Y.F.; Chen, J.F. *Stable Isotope Geochemistry*; Science Press: Beijing, China, 2000. (In Chinese)
36. Chen, J.P.; Zhao, C.Y.; Wang, Z.Y.; He, Z.H.; Qin, Y. Organic geochemical characteristics of oil, gas and source rocks of Jurassic coal measures in Northwestern China. *Geol. Rev.* **1998**, *44*, 149–159.

37. Chen, J.P.; Qin, Y.; Huff, B.G.; Wang, D.R.; Han, D.X.; Huang, D.F. Geochemical evidence for mudstone as the possible major oil source rock in the Jurassci Turpan Basin, Northwest China. *Org. Geochem.* **2001**, *32*, 1103–1125. [CrossRef]
38. Hoefs, J. *Stable Isotope Geochemistry*, 6th ed.; Springer: Göttingen, Germany, 2009.
39. Qiu, K.F.; Yu, H.C.; Deng, J.; McIntire, D.; Gou, Z.Y.; Geng, J.Z.; Chang, Z.S.; Zhu, R.; Li, K.N.; Goldfarb, R.J. The giant Zaozigou Au-Sb deposit in West Qinling, China:magmatic- or metamorphic-hydrothermal origin? *Miner. Depos.* **2020**, *55*, 345–362. [CrossRef]
40. Kirsten, S.; Habicht, D.E.; Canfield, J.; Rethmeier, G. Sulfur isotope fractionation during bacterial reduction and disproportionation of thiosulfate and sulfite. *Geochim. Cosmochim. Acta J. Geochem. Soc. Meteorit. Soc.* **1998**, *62*, 2585–2595.
41. Greenwood, P.F.; Mohammed, L.; Grice, K.; McCulloch, M.; Schwark, L. The application of compound-specific sulfur isotopes to the oil–source rock correlation of Kurdistan petroleum. *Org. Geochem.* **2018**, *117*, 22–30. [CrossRef]
42. Yin, J.; Xiang, W.D.; Ou, G.X.; Wang, Z.M.; Wang, X.Q. Microorganisms, organic matter, oil and gas and sandstone-type uranium deposits. *Uranium Geol.* **2005**, *21*, 287–295, 274. (In Chinese with English abstract)
43. Spirakis, C.S. The roles of organic matter in the formation of uranium deposits in sedimentary rocks. *Ore Geol. Rev.* **1996**, *11*, 53–69. [CrossRef]
44. Fuchs, S.H.; Schumann, D.; Williams-Jones, A.E.; Murray, A.J.; Couillard, M.; Lagarec, K.; Phaneuf, M.W.; Vali, H. Gold and uranium concentration by interaction of immiscible fluids (hydrothermal and hydrocarbon) in the Carbon Leader Reef, Witwatersrand Supergroup, South Africa. *Precambrian Res.* **2017**, *293*, 39–55. [CrossRef]

Disclaimer/Publisher's Note: The statements, opinions and data contained in all publications are solely those of the individual author(s) and contributor(s) and not of MDPI and/or the editor(s). MDPI and/or the editor(s) disclaim responsibility for any injury to people or property resulting from any ideas, methods, instructions or products referred to in the content.